Ship Detection From Raw SAR Echo Data

Xiangguang Leng, *Member, IEEE*, Kefeng Ji, *Member, IEEE*, and Gangyao Kuang, *Senior Member, IEEE*

***Abstract*— In the context of ship monitoring in the ocean, targets are usually sparsely distributed. Thus, synthetic aperture radar (SAR) imaging of the whole scene is usually quite redundant and costly. However, raw SAR echo data were considered to be useless before focusing. Few studies have attempted to detect ships from raw SAR echo data. It seems to be an impossible task since the resolution of raw SAR echo data is too low. This article proposes a ship detection method for raw SAR echo data in view of a nonimaging target sensing paradigm. The core idea is that we can sense the existence of ships from raw SAR echo data without imaging. The underlying rationale is that the radar always speaks the same sentence, i.e., usually an exactly identical linear frequency modulated (LFM) signal, while target and clutter answer differently. The difference spread into each part of the whole echo sequence rather than only the focused energy after match filtering. Thus, the ships can be found by pattern analysis on one-dimension sequence data rather than two-dimension images. The experimental results based on simulation and typical real data validate our assumption. This study shows that SAR imaging is an unnecessary intermediate process and opens up new significant possibilities for ship detection in the vast ocean.**

***Index Terms*— Raw echo data, ship detection, synthetic aperture radar (SAR).**

I. Introduction

SYNTHETIC aperture radar (SAR) is one of the great inventions in the history of remote sensing [1]. As an active sensor, it is famous for its 24-h all-weather imaging capabilities [2], [3]. SAR is unique and attractive for target detection since it works well when optical sensors suffer from night or cloud. SAR has been widely used in ocean monitoring since its invention. The traditional detection workflow includes three steps at least [4], [5], [6], [7], [8]. First, SAR produces a series of microwave pulses and records the backscattered echoes from the Earth. Then, the raw echo data are processed into focused SAR products by using the match filtering technique [9]. Finally, the focused products are fed into a detector to find out the target [10], [11], [12]. Since the invention of SAR, a concept has been widely accepted that the second step, i.e., imaging, is always essential and should be applied before detection. Almost all methods are applied to the focused detected [13], [14], [15], [16], [17], [18], [19], [20], [21] and single look complex (SLC) products [5], [6], [7], [8] or at least the range-compressed products [22], [23], [24], [25], [26]. For example, constant false alarm rate (CFAR) [18], [19], [20], [21], [22], [23] is one of the most widely used amplitude-based algorithms that is used to search for unusually brighter pixels than the surrounding sea clutter. The subaperture and higher order moment detectors can explore the value of using the spectral analysis technique [7] and complex-valued statistical information [5], [6], [8] in the SLC data. Recent methods based on convolutional neural networks (CNNs) [13], [14], [15], [16] can employ nonlinear deep visual features further. The reason to use focused data is also obvious. Without focus, the echo data are of very low spatial resolution. The energy of a point can spread into millions of pixels. Thus, traditional detectors fail to identify the existence of a target since it has a very low signal-to-clutter ratio (SCR). This traditional detection workflow and the underlying rationale are called the imaging target sensing paradigm in this article.

However, for present and future SAR missions, the imaging step and data transmission suffer from hard requirements caused by an increasing volume of data due to the large bandwidths, multiple channels, and wide-swath high-resolution. Though several new techniques are proposed to deal with this problem, e.g., sparse microwave imaging [27], they may degrade the image quality, discard or alternate the useful phase information of the moving ship targets, and involve massive computation. Besides, in the context of a detection mission, targets are usually sparsely distributed, especially for ships in the ocean. According to the statistics from United Nations Conference on Trade and Development (UNCTD) [28], there are approximately 100 000 oceangoing ships (100 gross tons and above) in total around the ocean of approximately 360 million km^2, i.e., approximately one ship per 3600 km^2. Thus, the imaging of the whole scene is usually quite redundant and costly when the SAR is used to monitor the ocean. Since raw SAR data acquisition is the primary and indispensable step in the whole workflow, prepositioning the detection step, i.e., sensing the target before imaging, maybe a potential solution to alleviate the burden of the subsequent steps and realize real instant target sensing.

It is intriguing to ask if we can detect ships from raw SAR data before imaging and only focus on the local region of interest to get rid of the redundant ocean background. To answer this question, it should be noted that, essentially, ship detection in SAR data belongs to a type of anomaly detection that exploits the backscattering responses of the target differing from the background. In general, to realize the detection, we must transform the SAR data domain into the detector domain to improve the SCR. The traditional focusing step, i.e., match filtering, is exactly such a process that focuses

Manuscript received 31 December 2022; revised 3 April 2023; accepted 27 April 2023. Date of publication 1 May 2023; date of current version 23 May 2023. This work was supported in part by the National Natural Science Foundation of China under Grant 62001480, in part by the Hunan Provincial Natural Science Foundation of China under Grant 2021JJ40684, and in part by the Research Funding of Satellite Information Intelligent Processing and Application Research Laboratory under Grant 2022-ZZKY-JJ-10-02. *(Corresponding author: Xiangguang Leng.)*

The authors are with the State Key Laboratory of Complex Electromagnetic Environment Effects on Electronics and Information System and the College of Electronic Science, National University of Defense Technology, Changsha 410073, China (e-mail: luckight@163.com).

This article has supplementary downloadable material available at https://doi.org/10.1109/TGRS.2023.3271905, provided by the authors.

Digital Object Identifier 10.1109/TGRS.2023.3271905

the energy of echoes to improve the SCR. However, it is noted that SCR is a concept in terms of the detector domain. In this case, its detector domain is mainly the focused two-dimension image or the mapping of this image. Actually, during this process, the total amount of information has not increased.

Though it seems difficult to use energy to distinguish ship target and sea clutter in raw SAR echo data, we can do it based on other detector domains wherein the SCR is high enough. This is natural if the radar echo is regarded as a kind of radar language, just like a bat. It is uncertain whether there is an imaging system in the bat's head. A proper assumption is that the bat needs no imaging system while it can recognize targets based on the echoes since it has very weak eyesight and has never seen imaging results before. On the contrary, the imaging system is needed by humans because they rely on their eyes for most spatial information. This supposes that the target can be found in the raw SAR echo data in a bat's way. In particular, an SAR sensor always speaks the same sentence, i.e., the coherent pulse, while the target and the clutter answer differently. The difference spread into each part of the whole sentence rather than only the focused energy after match filtering. Each sampling is a word of the echo. The whole sentence together can tell us whether there is a target.

This article proposes a new ship detection method in view of the nonimaging target sensing paradigm. The core idea is that we can sense targets from raw SAR echo data without imaging. The imaging step just needs to be applied to the local region of the target rather than the whole data which includes a large amount of redundant information. This operation is also called information bottleneck prepositioning in this article since the valid information is screened in advance. The experimental results based on simulation and typical real data validate our assumption. The main contribution of this article is concluded as follows.

1) A methodology of ship detection from raw SAR echo data is proposed. It takes into account both scattering and geometry characteristics of raw SAR data acquisition. The raw SAR echo data are treated as a one-dimension time sequence rather than a two-dimension matrix in this article.
2) The concept of a nonimaging target sensing paradigm is elaborated in this article. It breakthroughs the conventional practice that focusing must be applied before target detection. It shows that, in the context of target detection, imaging is an unnecessary intermediate process. Only raw SAR data acquisition and target detection are indispensable steps.
3) To the best of our knowledge, this is the first time wherein ship detection from raw SAR data is studied and completed in detail. The proposed idea may open up new possibilities for future target recognition based on SAR.

The remainder of this article is organized as follows. Section II reviews the raw SAR data acquisition model and proposes the nonimaging paradigm. A methodology of ship detection from raw SAR data is provided. Section III presents and discusses the experimental results based on simulation and real data. Section IV concludes this article.

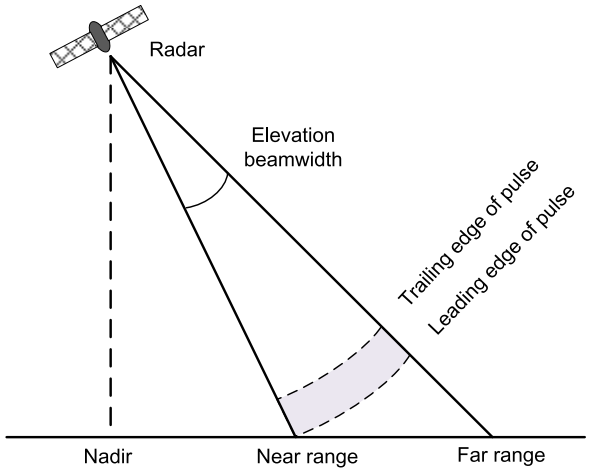

Fig. 1. Profile of pulse spreading outward.

II. Model and Methodology Description

In this section, at first, the raw SAR data acquisition model is presented to show the characteristics of raw SAR data. Then, the nonimaging target sensing paradigm is elaborated. The concept of information bottleneck prepositioning is also explained. Finally, the most important step in the paradigm, i.e., a complete methodology of ship detection from raw SAR echo data, is described in detail.

A. Raw SAR Data Acquisition Model

We consider the SAR signal first in the range direction. The commonly used pulse has a real-valued linear frequency modulated (LFM) characteristic

$$s_{\text{pul}}(\tau) = \omega_r(\tau)\cos\left(2\pi f_0\tau + \pi K_r\tau^2\right) \tag{1}$$

where $\omega_r(\cdot)$ is the range envelope, f_0 is the radar center frequency, K_r is the LFM rate, and τ is the fast time. As shown in Fig. 1, each point on the ground is illuminated by the beam for the pulse duration. At any instant, only a portion of the ground is illuminated. The echoes of each pulse are recorded in one-dimension storage.

As the radar advances along its path, as shown in Fig. 2, subsequent coherent pulses are transmitted and received at a precisely controlled time interval, i.e., the pulse repletion interval (PRI). Successive echoes are recorded in the subsequent rows. Thus, the raw data are arranged into a two-dimension matrix.

The radar carrier is removed before recording by quadrature demodulation usually. The demodulated signal of a single point target is represented as a complex-valued form [9]

$$\begin{aligned} s_0(\tau,\eta) \approx\ & A_0\omega_r\left[\tau - 2R(\eta)/c\right]\omega_a(\eta-\eta_c)\exp\{-j4\pi R_0/\lambda\} \\ & \times \exp\left\{-j4\pi K_a\eta^2\right\} \\ & \times \exp\left\{j\pi K_r(\tau - 2R(\eta)/c)^2\right\} \end{aligned} \tag{2}$$

where A_0 is a complex value (associated with the backscattering coefficient of the target), $\omega_a(\cdot)$ is the azimuth envelope, $R(\cdot)$ is the instant range, R_0 is the shortest range, A_0 is a slow time, and A_0 is the beam center crossing time. If A_0 is

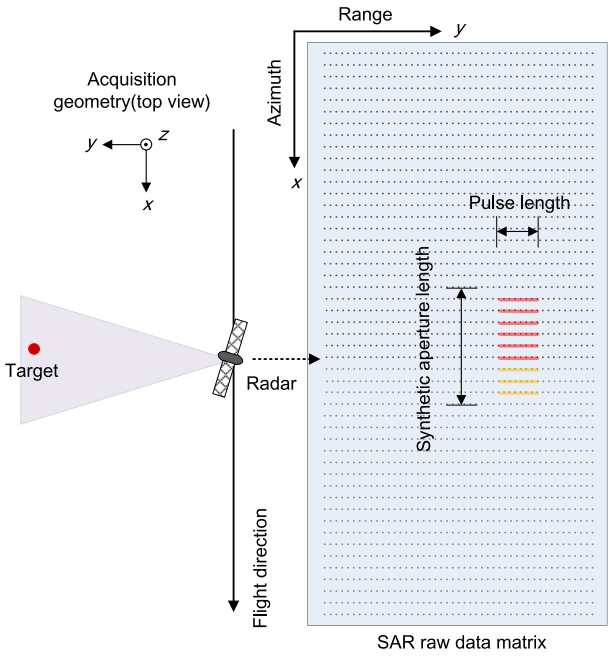

Fig. 2. Raw SAR data acquisition and arrangement.

ignored, we get the impulse response

$$h(\tau,\eta) \approx \omega_r\left[\tau - 2R(\eta)/c\right]\omega_a(\eta-\eta_c)\exp\{-j4\pi R_0/\lambda\} \times \exp\left\{-j4\pi K_a\eta^2\right\} \times \exp\left\{j\pi K_r(\tau - 2R(\eta)/c)^2\right\}. \quad (3)$$

Thus, the received signal from the ground, i.e., the raw SAR data, can be modeled as follows:

$$s_{\mathrm{bb}}(\tau,\eta) = g(\tau,\eta)\otimes h(\tau,\eta) + n(\tau,\eta) \quad (4)$$

where $g(\tau,\eta)$ represents the reflectivity of the ground and $n(\tau,\eta)$ represents the noise that can be ignored in the following analysis. As shown in Fig. 2, the extent of a target along the range direction in the raw SAR data is approximately the pulselength and along the azimuth direction the synthetic aperture length, separately. $g(\tau,\eta)$ is composed of two parts

$$\begin{aligned} s_{\mathrm{bb}}(\tau,\eta) &= (g_t(\tau,\eta) + g_c(\tau,\eta))\otimes h(\tau,\eta) + n(\tau,\eta) \\ &= g_t(\tau,\eta)\otimes h(\tau,\eta) + g_c(\tau,\eta)\otimes h(\tau,\eta) + n(\tau,\eta) \end{aligned} \quad (5)$$

where $g_t(\tau,\eta)$ and $g_c(\tau,\eta)$ represent the reflectivity of the target and the clutter background, respectively.

Though the raw SAR data are commonly treated as a two-dimension matrix, it can be seen that the raw SAR data are acquired in a one-dimension way. Besides, both directions can be modeled as an LFM signal. Thus, the raw SAR data can also be understood as the same kind of one-dimension signal in terms of the fast or slow time.

B. Nonimaging Paradigm

Fig. 3 shows the nonimaging target sensing paradigm (an animation chip is provided as the supplement file). It describes the complete workflow from raw SAR data acquisition to target focusing, which can be concluded as follows.

1) Acquiring Raw SAR Echo Data: As the radar advances, raw echoes are progressively collected. The radar beam should cover the scene that we want to observe. Raw SAR data used in the proposed paradigm can be the whole raw SAR data matrix after an imaging mission. It can also be the instant echo data during the acquisition.

2) Sensing Target From Raw SAR Data: The two-dimension raw SAR data are treated as a kind of sequence data. Since both directions can be modeled as an alike LFM signal, the two-dimension matrix can be expanded in terms of fast or slow time. For convenience, one-dimension sequence data in terms of the fast time are mainly considered in this article. The raw SAR data matrix of the target is screened by a target detection method based on a sequence model.

3) Focusing the Raw SAR Data Matrix of the Target: Once the raw SAR data matrix of the target is screened, they are focused by an imaging method, e.g., the range-Doppler (RD) method. Thus, a focused target chip that the human eyes can interpret is acquired.

As shown in Fig. 4, the input and the output of the proposed paradigm and the traditional one are the same. Data volume is reduced dramatically in the process and beneficial information for target detection is remained. Target detection can reject most redundant information thus this step can be treated as an information bottleneck. The main difference is that the proposed paradigm senses targets before imaging while the traditional one does it after imaging. This completes the information bottleneck prepositioning. Several points can be noted as follows.

1) The imaging step is not an information bottleneck since the total information is not reduced during imaging. It is only an information transformer that focuses the energy. It transforms the raw SAR echo data into a detector domain that is easy to interpret for human eyes.
2) Since the information contained in the raw SAR echo data is the same as the focused one, it is natural that we can detect targets in the raw SAR echo data once we use the proper way to deal with it. A two-dimension point target can be treated as a one-dimension sequence data.
3) Detecting targets from raw SAR echo data make the redundant information reduction in advance and thus, alleviates the computational burden of subsequent steps after the indispensable raw SAR data acquisition.

C. Ship Detection Methodology

This section first explains the detection rationale and then proposed the ship detection in the raw SAR echo data.

1) Detection Rationale: Since each echo line can be considered as a response of an LFM signal along the range and azimuth direction, we first only consider the one-dimension case along the range direction and ignore the modulation of the azimuth direction.

Each point on the ground is illuminated by the beam for the pulse duration. The pulse emitted for any point is the same and the echo difference of each point only depends on ground scatters. Each recorded echo is composed of the

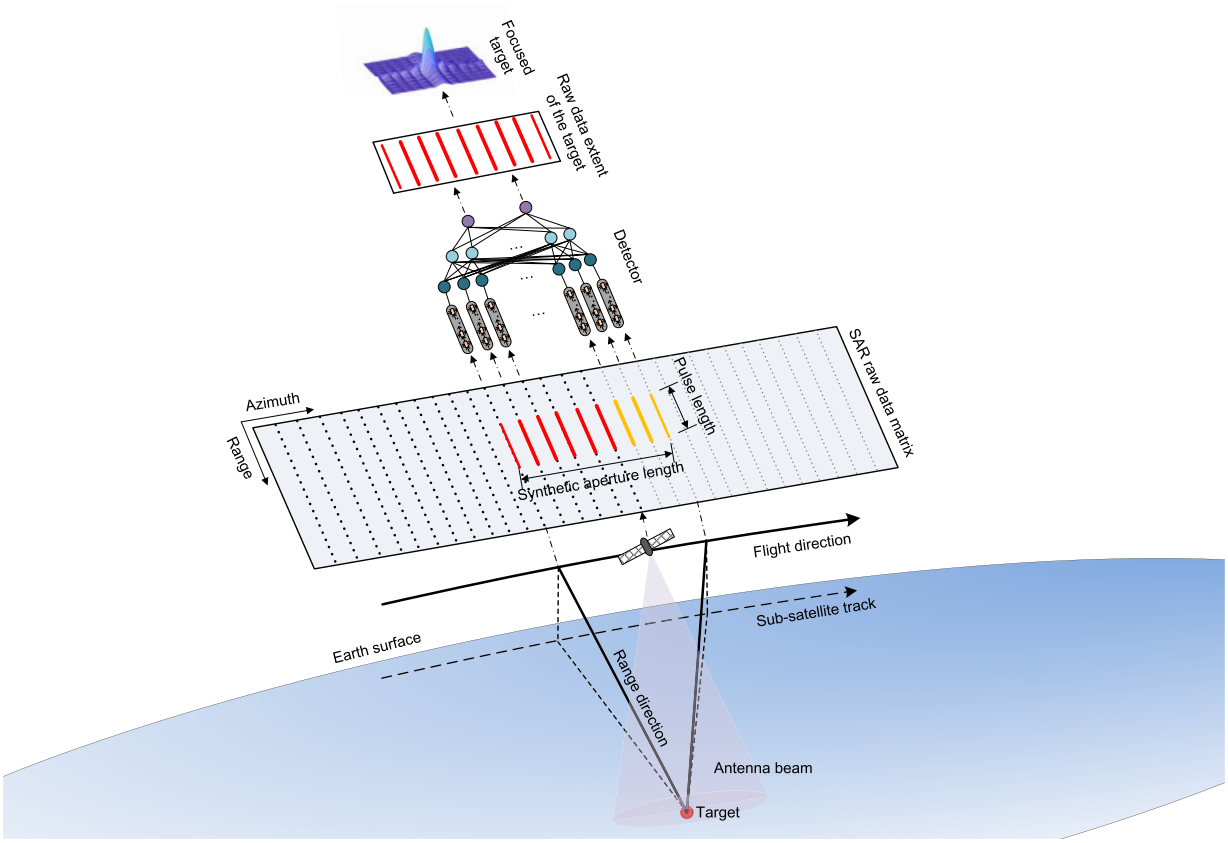

Fig. 3. Proposed nonimaging paradigm (an animation chip is provided as the supplement file).

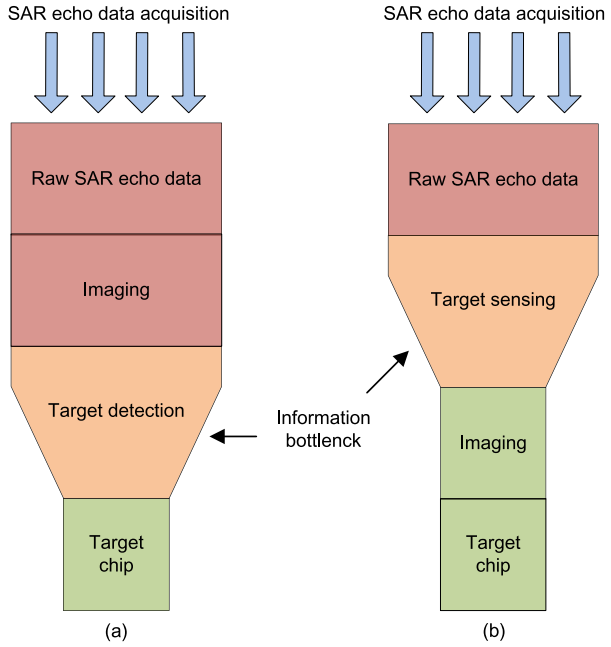

Fig. 4. (a) Comparison of the traditional paradigm and (b) nonimaging target sensing paradigm. It illustrates the valid information bottleneck prepositioning. The width of the graph represents the data volume roughly.

linear superposition of responses from the target and the clutter background. Since the scattering characteristic of a target is different from clutter, we consider that the mixed signal of the target and the clutter is also different from the signal of clutter. Let us view the SAR sensor and the scatters as if they are two persons, we would like to say that the SAR sensor always speaks the same sentence, while the target and the clutter answer differently. Thus, we can distinguish the target and clutter by the answer. However, different from the focused SAR image, the difference spread into each part of the whole echo rather than only the focused energy.

For a point target (indicating a target that is much stronger than the clutter and there is a dominant scattering), the echo can be modeled as

$$\begin{aligned} s_{\text{target}}(\tau) &= (g_t(\tau) + g_c(\tau)) \otimes h(\tau) + n(\tau) \\ &= g_t(\tau) \otimes h(\tau) + g_c(\tau) \otimes h(\tau) + n(\tau) \end{aligned} \tag{6}$$

where $g_t(\tau)$ and $g_c(\tau)$ represent the reflectivity of the target and the clutter background, respectively. $h(\tau)$ can be simplified as an LFM signal if we do not consider the two-way delay.

For the clutter, the echo can be modeled

$$\begin{aligned} s_{\text{clutter}}(\tau) &= g_c(\tau) \otimes h(\tau) + n(\tau) \\ &= \sum_{i=1}^{N} g_i(\tau) \otimes h(\tau) + n(\tau). \end{aligned} \tag{7}$$

Please note that the clutter is not a point target but many scatters. Thus, $g_c(\tau)$ can be decomposed into many $g_i(\tau)$ ($i = 1, 2, \ldots, N$, N is large enough). We set the reflectivity of the target as 1 and suppose that the reflectivity of clutter is much smaller than the point target. Thus, $g_c(\tau) \otimes h(\tau)$ can be modeled as a Gaussian distribution $g_{\text{gaussian}}(\tau)$ based

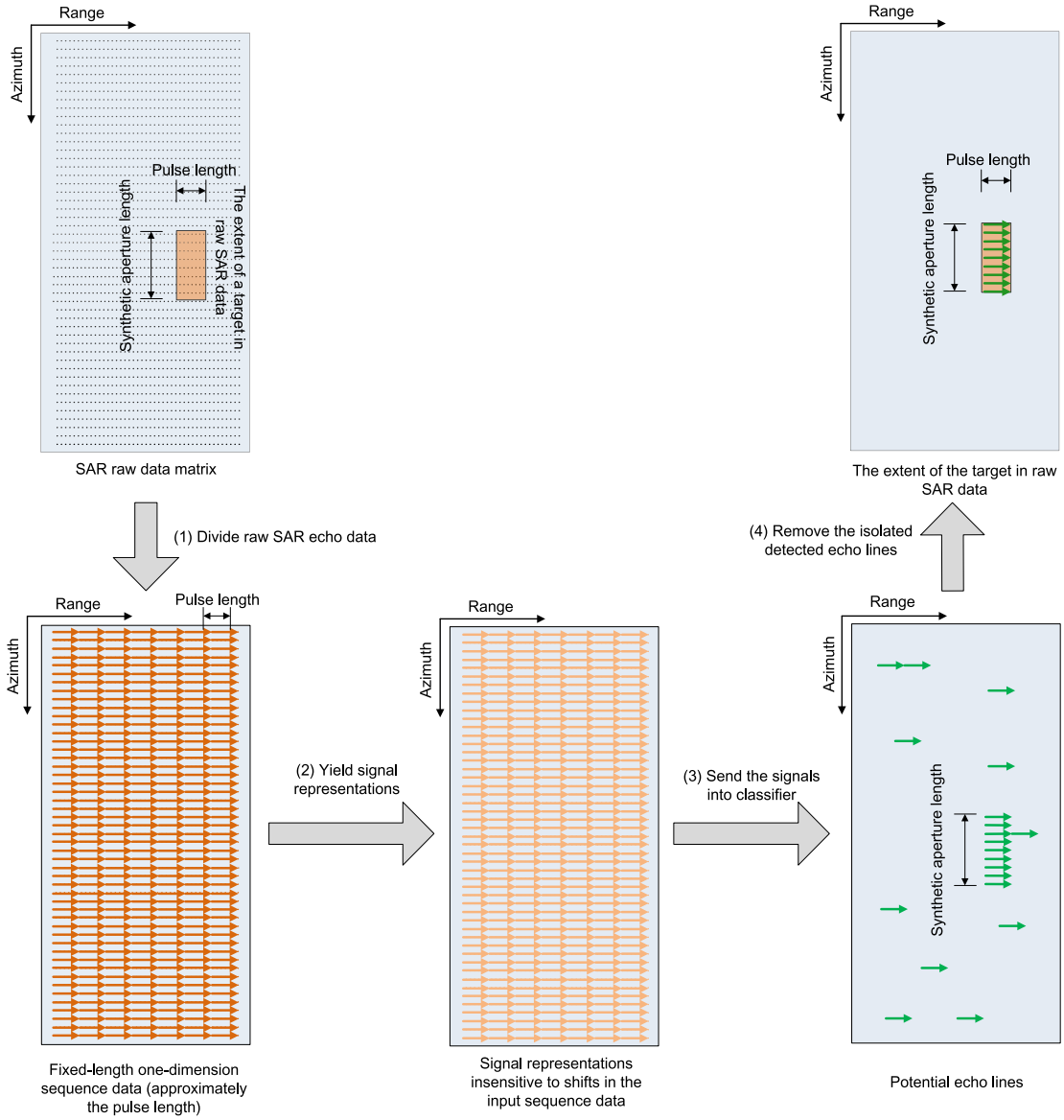

Fig. 5. Flowchart of the proposed ship detection method in raw SAR data.

on the central limit theorem. In addition, if $n(\tau)$ is ignored, (6) and (7) can be written as

$$s_{\text{target}}(\tau) = s_{\text{pul}}(\tau) + g_{\text{gaussian}}(\tau) \tag{8}$$

$$s_{\text{clutter}}(\tau) = g_{\text{gaussian}}(\tau). \tag{9}$$

Based on the above analyses, it can be known that to distinguish the point target and the clutter is approximately to distinguish the mixture of an LFM signal and a Gaussian clutter. The essence of detecting targets in the raw SAR echo data is to determine the extent of the target in the raw SAR echo data.

2) Proposed Method: Based on the analyses of the raw SAR data acquisition and the sensing rationale, we treat the raw SAR echo data as a kind of one-dimension sequence data. The detailed flowchart of the proposed method is shown in Fig. 5, which can be concluded as follows. It should be noted that the proposed method is designed for ship prescreening in open sea areas. Thus, the proposed method is more suitable for wide-swath and mid-resolution SAR images rather than high-resolution ones with smaller swaths.

3) Divide Raw SAR Data Into Fixed-Length One-Dimension Sequence Data: As shown in Fig. 5, we divide the raw SAR data into one-dimension sequence data. Since the extent of a target along the range direction in the raw SAR data is approximately the pulselength of a point target or half of the length, the one-dimension sequence data are divided into fixed-length groups. This would also help to reserve the entity of the scattering characteristics of the echo

$$s_{\text{bb}}(\varsigma) = g(\varsigma) \otimes h(\varsigma) + n(\varsigma) \tag{10}$$

where ς is a function of τ or A_0. For convenience, we mainly consider one-dimension sequence data in terms of the fast time, i.e., $\varsigma = \tau + N \times \text{PRI}$, N represents the location of the azimuth bin.

TABLE I
PARAMETERS OF BILSTM NETWORK ARCHITECTURE

Parameter	Value
Number of hidden units	100
Solver	Adam
Gradient threshold	1
Max epochs	200
Mini batch size	200

TABLE II
SIMULATION PARAMETERS FOR ONE-DIMENSION CASE

	Parameter	Value	Unit
For point target	Sampling frequency	$18.9e10^{6}$	s^{-1}
	Chip rate	$4.2e10^{11}$	s^{-2}
	Chip duration	$37.1e10^{-6}$	s
For clutter	Mean	0	
	Standard deviation	Variable	

4) Yield Signal Representations Insensitive to Shifts in the Input Sequence Data: Though the length of the echo group is the same as the pulselength, the leading and trailing points of the fixed-length group may not align with the true extent of the target. Thus, we need a feature extractor to alleviate or eliminate the influence caused by the shifts of the input echoes. In this article, the wavelet scattering feature (WCS) extractor [30] is adopted to deal with the real and imaginary parts of the input echoes, separately

$$\text{feature}(\varsigma) = \left[\text{WCS}(\text{real}(g(\varsigma))),\ \text{WCS}(\text{imag}(g(\varsigma)))\right]. \quad (11)$$

In this extractor, data are propagated through a series of wavelet transforms, nonlinearities, and averaging to produce low-variance representations of time series. The significant benefit of WCS is that it can yield signal representations insensitive to shifts in the input sequence data without sacrificing class discriminability. A wavelet scattering decomposition with two filter banks is used in this article. Eight wavelets per octave are in the first filter bank and one wavelet per octave is in the second filter bank. The invariance scale is set to the length of the data, i.e., the pulselength.

5) Send the Signal Representations Into a Classifier to Find Out the Potential Echo Lines: The aim of the classifier is to determine if the echoes of the fixed length contain responses from the target. Thus, it is actually a binary classification. Since the echo along the range direction is taken as a kind of radar language, it can be naturally processed by a natural language processing method. As a kind of recurrent neural network (RNN) architecture that can learn long-term dependencies, long short-term memory (LSTM) [31], [32] is an effective way to find out responses from the target in the radar echoes. In this article, a bidirectional LSTM, or BiLSTM is adopted to classify the echo data, since it can increase the amount of information available to the network, improving the context. A BiLSTM consists of two LSTMs: one taking the input in a forward direction and the other in a backward direction, which has been widely used to solve a number of sequence learning problems. The parameters of the BiLSTM network architecture are listed in Table I.

The output of the BiLSTM can be written as follows:

$$\text{if BiLSTM}(\text{feature}(\varsigma)) = \begin{cases} 1, & \text{then } s_{\text{bb}}(\varsigma) \text{ contains} \\ & \text{responses from target} \\ 0, & \text{then } s_{\text{bb}}(\varsigma) \text{does not} \\ & \text{contain responses from target.} \end{cases} \quad (12)$$

After all echo lines are fed into the BiLSTM, as shown in Fig. 5, the final output of BiLSTM is the potential echo lines that contain the responses from the target.

6) Remove the Isolated Detected Echo Lines and Acquire Successive Echo Lines of the Target: Due to the diversity of the clutter background, e.g., numerous erratic spikes, some responses of the clutter may be very similar to the target. Thus, the output of BiLSTM may contain false alarms caused by the cluttered background. However, it is realized that the similarity between the clutter and the target is not stable. The responses of the clutter vary during the synthetic aperture time while this is not true for the target. Thus, most echoes of the target during the synthetic aperture time should be detected while most echoes of clutter are not detected. That is to say, as shown in Fig. 5, the detected echoes of a target are approximately successive along the azimuth direction and the length is approximately the synthetic aperture length. On the contrary, the detected echoes of clutter are isolated. Thus, we can filter all the potential echo lines and remove the isolated ones. This can be implemented by a density filter along the azimuth direction. Finally, only the successive part along the azimuth direction is remained. This section represents the extent of the target in the raw SAR data.

III. EXPERIMENTAL RESULTS AND ANALYSES

In this section, the experimental results acquired by the proposed method are introduced and analyzed. To validate the performance of the proposed method, both simulation and real datasets are tested. The first and the second parts of this section introduce the results based on simulation and real datasets, respectively. Note that the proposed method is mainly designed to detect ships in the background of a vast ocean, thus only typical real data of open ocean scenes are presented in this article.

A. Experiments Based on Simulation Data

Table II lists the typical simulation parameters for the one-dimension case. This is the most fundamental and meaningful case. The LFM parameters for a point target are similar to the spaceborne SAR configuration (e.g., ERS-2). The mean value for the clutter amplitude is set as 0 which is consistent with the real situation. The standard deviation is variable to simulate different clutter levels with different SCRs. Based on the parameters, we can get a lot of random echoes to simulate the real world. Fig. 6 shows a typical simulation result (the standard deviation is 2 here, corresponding that the SCR is

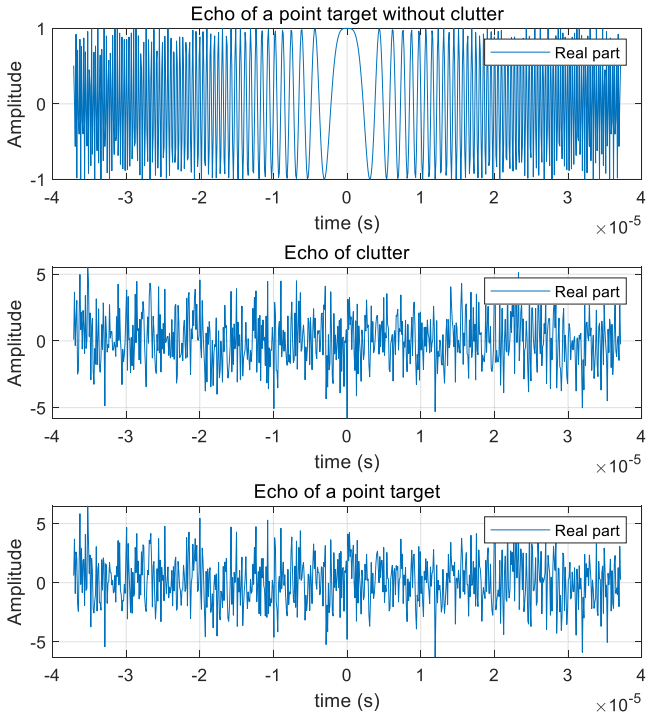

Fig. 6. Echo simulation results of a one-dimension case.

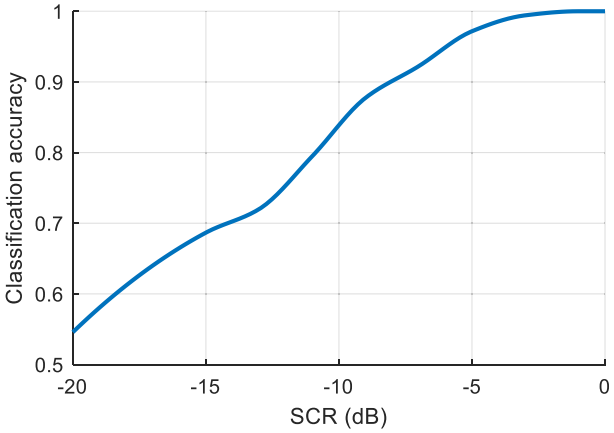

Fig. 7. Classification accuracy under different SCRs.

approximately –6 dB). The first row presents the echo of a pure point target without clutter. The second row presents the echo of clutter. The bottom row presents the echo of a point target mixed with the clutter. It can be seen that the echo of a point target is very similar to the clutter. They both seem to be chaotic and cannot be distinguished by the human eyes.

In this article, we set several different kinds of SCRs by adjusting the standard deviation. For each SCR, a total of 1200 random echoes of clutter and 1200 random echoes of targets are produced. Half of the simulation results are used to train the network and half are used to test. For each SCR, we can get a classification accuracy, thus we can finally get an accuracy curve in terms of the SCR.

Fig. 7 shows the classification accuracy under different SCRs. The accuracy is defined as

$$\text{accuracy} = (TP + TN)/(P + N) \tag{13}$$

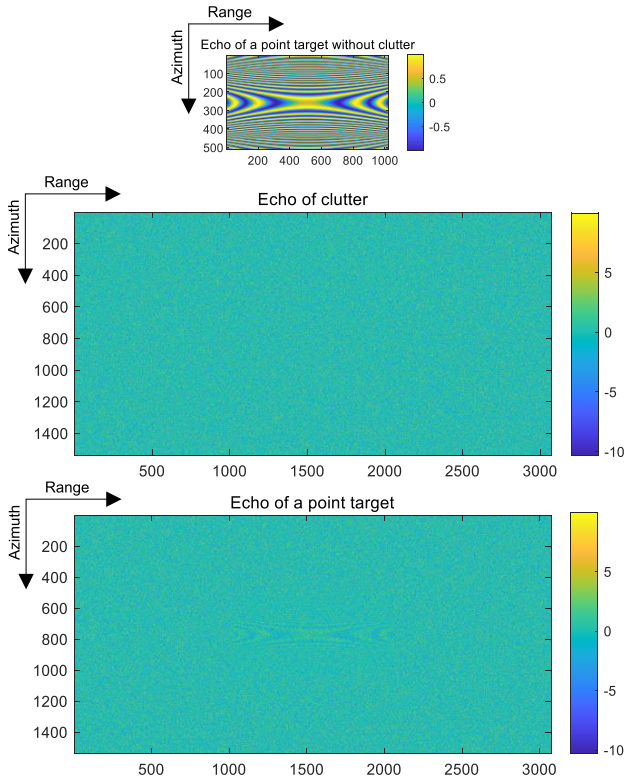

Fig. 8. Echo simulation results (real part) of a two-dimension case.

where TP and TN represent the numbers of the detected true positive echo lines and the detected true negative echo lines, respectively. P and N represent the numbers of positive and negative echo lines, i.e., the ground truth, respectively.

Based on this one-dimension case, we would know the potential baseline for distinguishing the two kinds of echoes. The classification accuracy decreases as SCR decreases. This is natural because when SCR decreases, the signature of the target signal is flooded by the clutter signal. It can be seen that when the SCR is high (>–5 dB, corresponding to the clutter standard deviation is 1.8 times the signal amplitude), the accuracy can be very high (larger than 95%). When the SCR reaches –20 dB (corresponding to that the clutter standard deviation is ten times the signal amplitude), the accuracy approaches 50% (a meaningless result of binary classification). Actually, it should be noted that when the SCR reaches –20 dB (a very bad situation), even after the matched filtering the target can be also not distinguishable. This implies that the performance would be degraded by the high dynamic background, small target, and other possible cases. If a classification accuracy above 80% is needed, the experimental results suggest that the SCR should be >–11 dB (corresponding to that the clutter standard deviation is 3.5 times the signal amplitude).

The 2-D case is similar to the one-dimension one. The simulation parameters are shown in Table III. The parameters for the point target are also similar to the ERS-2 spaceborne SAR configuration and the azimuth parameters are taken into consideration in addition. The standard deviation of the two-dimension random matrix is set as 2. Fig. 8 shows an illustration of a two-dimension simulation case. We use the

TABLE III
SIMULATION PARAMETERS FOR TWO-DIMENSION CASE

	Parameter	Value	Unit
For point target	Range sampling frequency	$150e10^{6}$	s^{-1}
	Chip rate	$5e10^{12}$	s^{-2}
	Chip duration	$30e10^{-6}$	s
	Velocity	$7e^{3}$	m/s
	Wavelength	0.056	m
	Initial slant range	$800e^{3}$	m
	Aperture time	0.6	s
	Pulse repetition frequency	1700	s^{-1}
For clutter	Mean	0	
	Standard deviation	2	

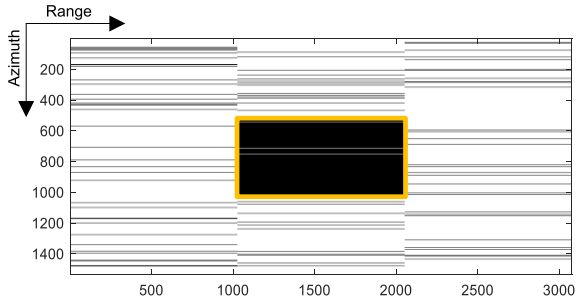

Fig. 9. Sensing results of the two-dimension raw echo matrix. The black lines represent the potential echo lines of the point target. The yellow rectangle represents the detected target extent.

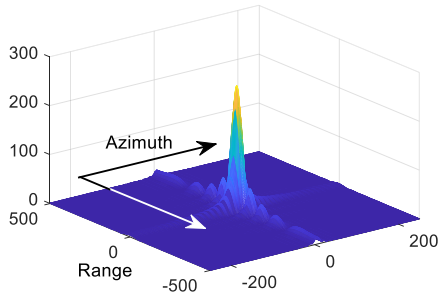

Fig. 10. Focused result of detection extent of the point target.

superposition of a pure point target and a two-dimension random matrix that follows a Gaussian distribution to simulate a point target. The first, second, and bottom rows present the echoes of a pure point target without clutter, the clutter, and the point target mixed with the clutter. The size of the two-dimension random matrix is three times larger and aligns with the center of the point target.

The sensing result is shown in Fig. 9. It can be seen that most of the echo lines of the point target are detected by the proposed method. Though there are some false alarms caused by clutter, the extent of the point target can be easily found since the false alarms are sparser. This is in accordance with the expectation. An approximate accuracy of 93.8% is achieved in this case. Most of the clutter echoes are rejected, and thus, the imaging step is able to only focus on the target. Fig. 10 shows the focused result of the point target.

B. Experiments Based on Typical Real Data

This section selects two typical scenes to validate the effectiveness of the proposed method. One is the data from ERS-2 and the other one is from Gaofen-3.

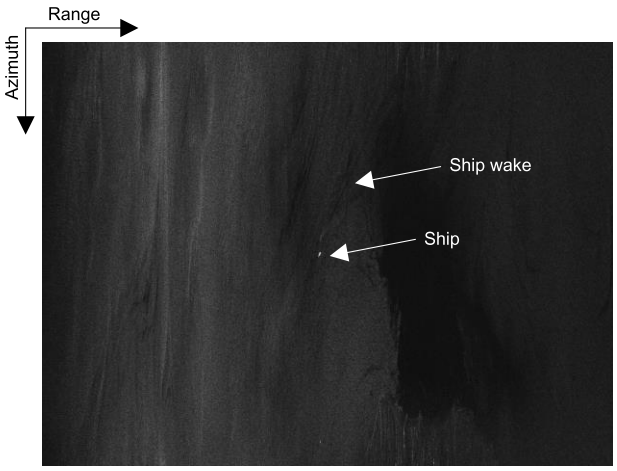

Fig. 11. Focused ERS-2 SAR data. There is a ship in the center.

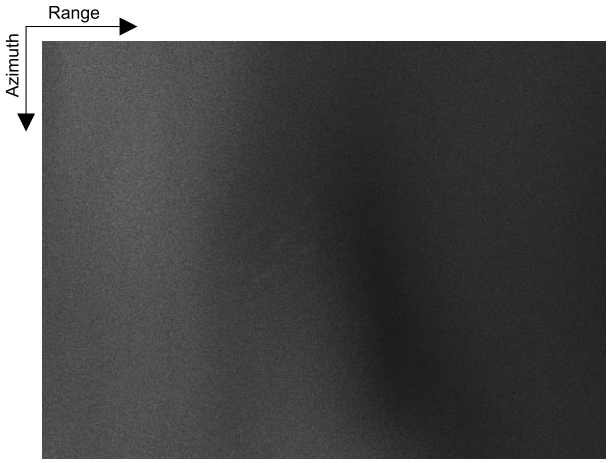

Fig. 12. Unfocused ERS-2 raw echo data.

1) ERS-2 STD Data With Land Areas: Fig. 11 shows a focused ERS-2 SAR amplitude image. It was acquired in VV polarization and C- band. The imaging mode is STD with a spatial resolution of approximately 25 m. The imaging parameters are similar to the ones presented in the two-dimension simulation case. The wake in Fig. 11 demonstrates that the bright target in the center is a moving ship. Fig. 12 shows the corresponding raw echo data. It can be seen that the echoes of the ship are flooded by the clutter. The ship cannot be identified in the raw SAR data by human eyes. All details are hidden in the echoes. Note that there are land areas at the bottom right in this scene. Based on the proposed method, Fig. 13 presents the sensing results. It can be seen from the result that most echo lines of the ship are detected by the proposed method and most redundant clutter is rejected. An approximate accuracy of 83.3% is achieved in this case. Compared to the simulation case, the accuracy achieved based on real data decreases due to the false alarms caused by the land areas at the bottom right and sea clutter at the right. The region of interest, i.e., the extent of the ship target can be easily determined and is focused. Finally, as shown in Fig. 14, we can get the focused ship target without imaging the whole scene. Irrelevant information is prescreened in advance.

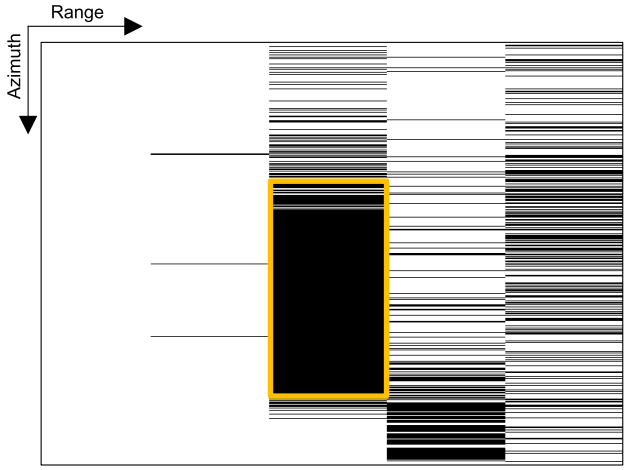

Fig. 13. Detection results of ERS-2 raw echo data. The black lines represent the potential echo lines of the ship target. The yellow rectangle represents the detected target extent.

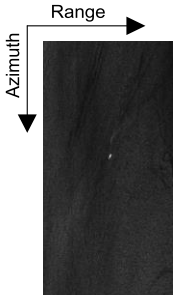

Fig. 14. Focused result of the detected extent in ERS-2 raw echo data.

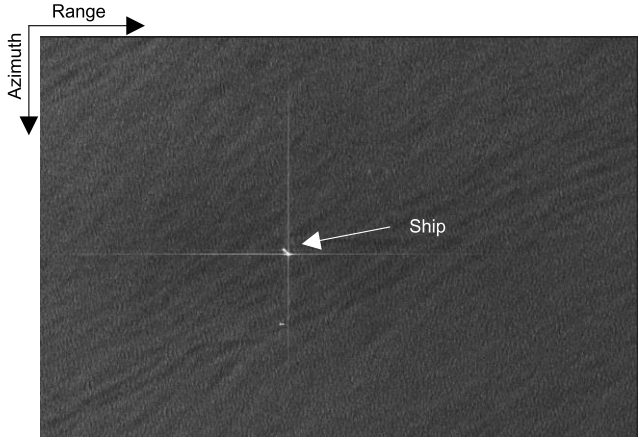

Fig. 15. Focused Gaofen-3 FSI data. There is a ship in the center.

2) Gaofen-3 FSI Data With Pure Sea: The second scene comes from Gaofen-3. As shown in Fig. 15, there is a ship in the center of the scene. This scene is acquired by the Gaofen-3 Fine StripMap I (FSI) mode and HH polarization. The resolution is approximately 5 m. The imaging parameters are listed in Table IV. Compared to the previous ERS-2 data, there are no land areas and the resolution is higher. Different from the ERS-2 data, the raw data of the ship target are stronger than the sea clutter. As shown in Fig. 16, the echoes of the ship can be identified by human eyes in this case. This may be caused by the fact that the amplitude of the ship in Gaofen-3

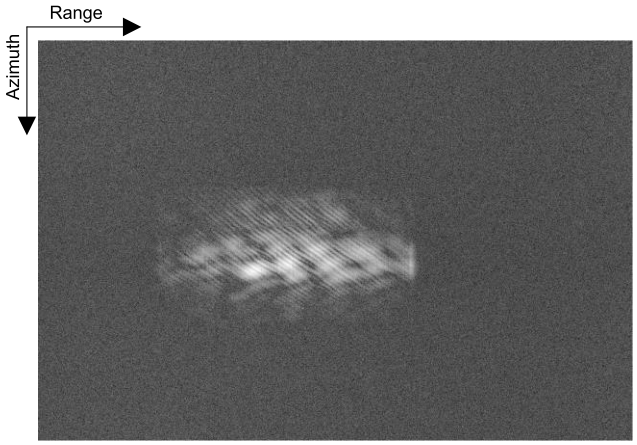

Fig. 16. Unfocused Gaofen-3 FSI raw echo data.

TABLE IV
IMAGING PARAMETERS FOR GAOFEN-3 FSI MODE

Parameter	Value	Unit
Range sampling frequency	$133e10^{6}$	s^{-1}
Chip rate	$4e10^{12}$	s^{-2}
Chip duration	$30e10^{-6}$	s
Velocity	$7e^{3}$	m/s
Wavelength	0.056	m
Initial slant range	$800e^{3}$	m
Pulse repetition frequency	2537	s^{-1}

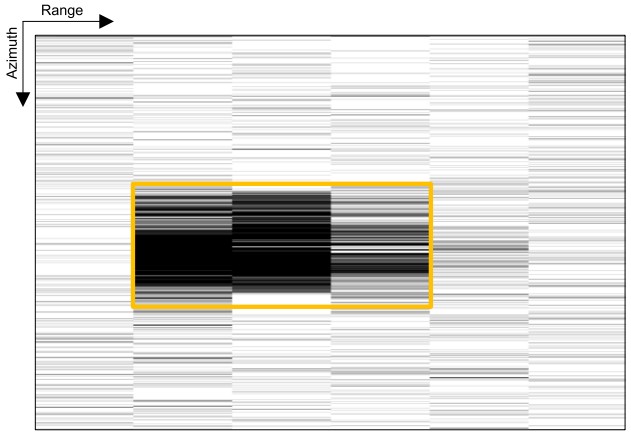

Fig. 17. Detection results of Gaofen-3 FSI raw echo data. The black lines represent the potential echo lines of the ship target. The yellow rectangle represents the detected target extent.

FSI mode is much stronger than the sea clutter. This can be acknowledged by that in the focused image the amplitude of the ship is approximately thousands of times stronger than the sea clutter in Gaofen-3 FSI mode while dozens of times in ERS-2 data. Fig. 17 shows the detection results of the proposed method. It can be seen that the proposed method can found the extent of the echoes of the ship target. Though there are some false detected lines in the detected results, they can be removed since they are not successive. Based on the successive detected region in the results, we can get the focused ship target directly, as shown in Fig. 18.

In the above experiments, we only present the detection results along the range direction. Actually, as we mentioned in the method introduction, it can be also applied along the

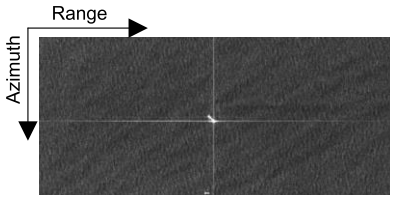

Fig. 18. Focused result of the detected extent in Gaofen-3 data.

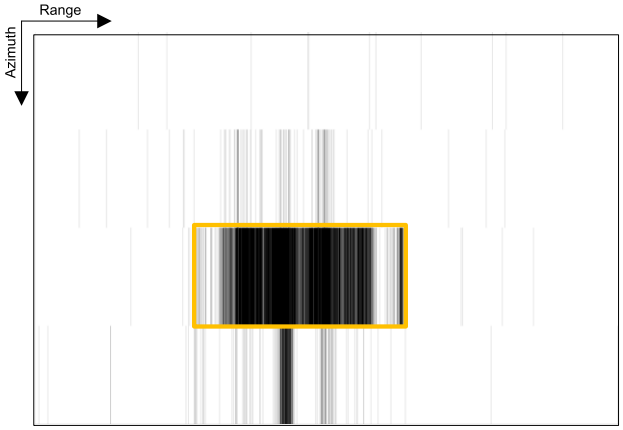

Fig. 19. Detection results of Gaofen-3 FSI raw echo data along the azimuth direction. The black lines represent the potential echo lines of the ship target. The yellow rectangle represents the detected target extent.

azimuth direction. Fig. 19 shows the results we get along the azimuth direction. It can be seen that the detection results are similar to the one along the range direction with negligible error.

C. Discussions

For a long time, target detection from raw SAR echo data has been considered to be an impossible task since the resolution of raw SAR data is too low and the energy of the target and clutter background are mixed. Raw SAR data are always focused before target detection. This article uses typical experimental data to demonstrate that this conventional practice may be not true. We provided a new methodology based on the analyses of the pattern in one-dimension sequence data rather than the traditional two-dimension images. Experimental results demonstrate that the proposed method can achieve the desired effect to find out the extent of a ship in the vast ocean. This may be of great importance for the alleviation of the computation and storage burden on board and the realization of real instant target sensing or cognitive SAR.

It is noted that SAR microwave vision [33], [34] is a novel concept and hotspot that tries to recognize targets by referring to human brain vision perception mechanism and computer vision-related technology, integrating electromagnetic physical law and radar imaging mechanism. The proposed method tries to detect ships from raw SAR data by taking into account both scattering and geometry characteristics of raw SAR data acquisition. Each echo is treated as a special radar language and sensed together. Thus, the proposed method can be regarded as a representative target detection approach of microwave vision.

However, note that in this article, only ideal or simple scenes are taken into consideration. i.e., there is usually only an isolated ship in the scene surrounded by pure sea clutter. The real scene may be much more complicated than the typical scenes presented in the experiments, e.g., there may be several ships in the scene or the ship may be polluted by other interference. Besides, if the ship is too weak in the echoes, it may be not detectable by the proposed method. In sum, the proposed method may fail to deal with more complicated cases. Besides, there is no comparison presented in this article due to the lack of similar research studies. It should also be noted that the ocean background is important for some other applications, such as wind retrieval. However, the ocean background is considered as useless since this article mainly focuses on ship detection.

IV. Conclusion

In summary, this article proposed a ship detection method from raw SAR echo data without the imaging step. It tries to detect ships directly from the raw SAR echo data to get rid of redundant imaging of the sea clutter background. In the proposed method, each echo of the target is treated as a special radar language and sensed together. Demonstrations based on simulation data and typical real data validate the idea. This perspective breaks through the traditional idea that target detection must be operated in the focused SAR product though the proposed method was tested in a pure sea background. This may expand understanding and promising applications of target detection based on SAR data. We believe that our approach would be a significant outcome to uses SAR to recognize targets. In the future, more works would be applied to the adaptability of the method.

Acknowledgment

The authors would like to thank the ASF website for providing free ERS-2 data.

References

[1] A. Moreira, P. Prats-Iraola, M. Younis, G. Krieger, I. Hajnsek, and K. P. Papathanassiou, "A tutorial on synthetic aperture radar," *IEEE Geosci. Remote Sens. Mag.*, vol. 1, no. 1, pp. 6–43, Mar. 2013.

[2] D. Massonnet et al., "The displacement field of the Landers earthquake mapped by radar interferometry," *Nature*, vol. 364, no. 6433, pp. 138–142, 1993.

[3] C. Enderli, L. Savy, and P. Refregier, "Application of the deflection criterion to classification of radar SAR images," *IEEE Trans. Pattern Anal. Mach. Intell.*, vol. 29, no. 9, pp. 1668–1672, Sep. 2007.

[4] A. Filippidis, L. C. Jain, and N. Martin, "Fusion of intelligent agents for the detection of aircraft in SAR images," *IEEE Trans. Pattern Anal. Mach. Intell.*, vol. 22, no. 4, pp. 378–384, Apr. 2000.

[5] X. Leng, K. Ji, S. Zhou, and X. Xing, "Ship detection based on complex signal kurtosis in single-channel SAR imagery," *IEEE Trans. Geosci. Remote Sens.*, vol. 57, no. 9, pp. 6447–6461, Sep. 2019.

[6] Z. Lv, J. Lu, Q. Wang, Z. Guo, and N. Li, "ESP-LRSMD: A two-step detector for ship detection using SLC SAR imagery," *IEEE Trans. Geosci. Remote Sens.*, vol. 60, 2022, Art. no. 5233516.

[7] A. Marino, M. J. Sanjuan-Ferrer, I. Hajnsek, and K. Ouchi, "Ship detection with spectral analysis of synthetic aperture radar: A comparison of new and well-known algorithms," *Remote Sens.*, vol. 7, no. 5, pp. 5416–5439, Apr. 2015.

[8] X. Leng, K. Ji, S. Zhou, X. Xing, and H. Zou, "Discriminating ship from radio frequency interference based on noncircularity and non-Gaussianity in Sentinel-1 SAR imagery," *IEEE Trans. Geosci. Remote Sens.*, vol. 57, no. 1, pp. 352–363, Jan. 2019.

[9] I. Cumming and F. Wong, *Digital Signal Processing of Synthetic Aperture Radar Data: Algorithms and Implementation*. Norwood, MA, USA: Artech House, 2004.

[10] K. El-Darymli, E. W. Gill, P. Mcguire, D. Power, and C. Moloney, "Automatic target recognition in synthetic aperture radar imagery: A state-of-the-art review," *IEEE Access*, vol. 4, pp. 6014–6058, 2016.

[11] D. J. Crisp, "The state-of-the-art in ship detection in synthetic aperture radar imagery," DSTO Inf. Sci. Lab., Edinburgh, SA, Australia, Tech. Rep. RR-0272, May 2004.

[12] O. Kechagias-Stamatis and N. Aouf, "Automatic target recognition on synthetic aperture radar imagery: A survey," *IEEE Aerosp. Electron. Syst. Mag.*, vol. 36, no. 3, pp. 56–81, Mar. 2021.

[13] Q. An, Z. Pan, and H. You, "Ship detection in Gaofen-3 SAR images based on sea clutter distribution analysis and deep convolutional neural network," *Sensors*, vol. 18, no. 2, p. 334, 2018.

[14] J. Cui, H. Jia, H. Wang, and F. Xu, "A fast threshold neural network for ship detection in large-scene SAR images," *IEEE J. Sel. Topics Appl. Earth Observ. Remote Sens.*, vol. 15, pp. 6016–6032, 2022, doi: 10.1109/JSTARS.2022.3192455.

[15] B. Hou et al., "A neural network based on consistency learning and adversarial learning for semisupervised synthetic aperture radar ship detection," *IEEE Trans. Geosci. Remote Sens.*, vol. 60, 2022, Art. no. 5220816, doi: 10.1109/TGRS.2022.3142017.

[16] Z. Zhou, Z. Cui, Z. Cao, and J. Yang, "Feature-transferable pyramid network for dense multi-scale object detection in SAR images," in *Proc. IEEE Int. Geosci. Remote Sens. Symp. (IGARSS)*, Jul. 2022, pp. 647–650.

[17] P. Iervolino and R. Guida, "A novel ship detector based on the generalized-likelihood ratio test for SAR imagery," *IEEE J. Sel. Topics Appl. Earth Observ. Remote Sens.*, vol. 10, no. 8, pp. 3616–3630, Aug. 2017.

[18] C. Santamaria, M. Alvarez, H. Greidanus, V. Syrris, P. Soille, and P. Argentieri, "Mass processing of Sentinel-1 images for maritime surveillance," *Remote Sens.*, vol. 9, no. 7, p. 678, Jul. 2017.

[19] H. Greidanus and C. Santamaria, "First analyses of Sentinel-1 images for maritime surveillance," Publications Office Eur. Union, Luxembourg, JRC Sci. Policy Rep. JRC92666 and EUR 27031 EN, 2014, doi: 10.2788/132810.

[20] X. Leng, K. Ji, K. Yang, and H. Zou, "A bilateral CFAR algorithm for ship detection in SAR images," *IEEE Geosci. Remote Sens. Lett.*, vol. 12, no. 7, pp. 1536–1540, Jul. 2015.

[21] X. Leng, K. Ji, X. Xing, S. Zhou, and H. Zou, "Area ratio invariant feature group for ship detection in SAR imagery," *IEEE J. Sel. Topics Appl. Earth Observ. Remote Sens.*, vol. 11, no. 7, pp. 1–13, Apr. 2018.

[22] S. K. Joshi and S. V. Baumgartner, "Automatic CFAR ship detection in single–channel range-compressed airborne radar data," in *Proc. 20th Int. Radar Symp. (IRS)*, Jun. 2019, pp. 1–8.

[23] S. K. Joshi, S. V. Baumgartner, A. B. C. Silva, and G. Krieger, "Range-Doppler based CFAR ship detection with automatic training data selection," *Remote Sens.*, vol. 11, no. 11, pp. 1270-1–1270-39, 2019, doi: 10.3390/rs11111270.

[24] S. K. Joshi, S. V. Baumgartner, and G. Krieger, "Tracking and track management of extended targets in range-Doppler using range-compressed airborne radar data," *IEEE Trans. Geosci. Remote Sens.*, vol. 60, 2022, Art. no. 5102720.

[25] X. Leng, J. Wang, K. Ji, and G. Kuang, "Ship detection in range-compressed SAR data," in *Proc. IEEE Int. Geosci. Remote Sens. Symp. (IGARSS)*, Jul. 2022, pp. 2135–2138, doi: 10.1109/IGARSS46834.2022.9884909.

[26] T. Loran, A. B. C. D. Silva, S. K. Joshi, S. V. Baumgartner, and G. Krieger, "Ship detection based on faster R-CNN using range-compressed airborne radar data," *IEEE Geosci. Remote Sens. Lett.*, vol. 20, pp. 1–5, 2023, doi: 10.1109/LGRS.2022.3229141.

[27] Y. Wu, "Study on sparse microwave imaging," in *Proc. IEEE CIE Int. Conf. Radar*, Oct. 2011, p. 9.

[28] UNCTAD. *Review of Maritime Transport 2022*. Accessed: Nov. 30, 2022. [Online]. Available: https://unctad.org/webflyer/review-maritime-transport-2022

[29] X. Leng, K. Ji, and G. Kuang, "First demonstration of using raw SAR data for target detection," in *Proc. IGARSS* 2023, pp. 1–2.

[30] M. J. Vrhel, C. Lee, and M. Unser, "Rapid computation of the continuous wavelet transform by oblique projections," *IEEE Trans. Signal Process.*, vol. 45, no. 4, pp. 891–900, Apr. 1997.

[31] S. Hochreiter and J. Schmidhuber, "Long short-term memory," *Neural Comput.*, vol. 9, no. 8, pp. 1735–1780, 1997.

[32] O. Koller, N. C. Camgoz, H. Ney, and R. Bowden, "Weakly supervised learning with multi-stream CNN-LSTM-HMMs to discover sequential parallelism in sign language videos," *IEEE Trans. Pattern Anal. Mach. Intell.*, vol. 42, no. 9, pp. 2306–2320, Sep. 2020.

[33] F. Xu and Y. Jin, "From the emergence of intelligent science to the research of microwave vision," *Sci. Technol. Rev.*, vol. 36, no. 10, pp. 30–44, 2018.

[34] Y. Jin, "Multimode remote sensing intelligent information and target recognition: Physical intelligence of microwave vision," *J. Radars*, vol. 8, no. 6, pp. 710–716, 2019.

Xiangguang Leng (Member, IEEE) received the B.S. degree in remote sensing science and technology from Wuhan University (WHU), Wuhan, China, in 2013, and the M.S. degree (Hons.) in photogrammetry and remote sensing and the Ph.D. degree in electronic science and technology from the National University of Defense Technology (NUDT), Changsha, China, in 2015 and 2019, respectively.

He is currently an Associate Professor at the College of Electronic Science and Technology, NUDT. His research interests mainly include remote sensing information processing, synthetic aperture radar (SAR) image interpretation, and machine learning.

Dr. Leng was a recipient of the Excellent Doctoral Dissertation of Hunan Province and China Education Society of Electronics, the Best Report Award from the First Doctoral Forum of *Journal of Radars*, the Excellent Paper Award from the 2016 CIE International Conference on Radar, the 2018 IET International Radar Conference, and the 5th China High Resolution Earth Observation Conference. He is a reviewer of several international journals.

Kefeng Ji (Member, IEEE) received the B.S. degree in aerospace engineering from Northwestern Polytechnical University (NWPU), Xi'an, China, in 1996, and the M.S. and Ph.D. degrees in information and telecommunication engineering from the National University of Defense Technology (NUDT), Changsha, China, in 1999 and 2003, respectively.

In 2003, he joined the College of Electronic Science, NUDT, where he is currently a Professor. He has authored or coauthored over 80 articles. His research interests include signal processing, machine learning, pattern recognition, remote sensing information processing, synthetic aperture radar (SAR) image interpretation, target detection, recognition, feature extraction, and marine surveillance.

Dr. Ji is a reviewer of several international journals and conferences, such as IEEE TRANSACTIONS ON GEOSCIENCE AND REMOTE SENSING, IEEE JOURNAL OF SELECTED TOPICS IN APPLIED EARTH OBSERVATIONS AND REMOTE SENSING, IEEE GEOSCIENCE AND REMOTE SENSING LETTERS, IEEE ACCESS, IEEE TRANSACTIONS ON INDUSTRIAL INFORMATICS, *International Journal of Remote Sensing*, *Remote Sensing Letters*, *European Journal of Remote Sensing*, and *Remote Sensing*.

Gangyao Kuang (Senior Member, IEEE) received the B.S. and M.S. degrees in geophysics from the Central South University of Technology, Changsha, China, in 1988 and 1991, respectively, and the Ph.D. degree in communication and information from the National University of Defense Technology (NUDT), Changsha, in 1995.

He is currently a Professor with the College of Electronic Science, NUDT. His research interests include remote sensing, synthetic aperture radar (SAR) image processing, change detection, SAR ground moving target indication, and classification with polarimetric SAR images.